2020

Spin-torque switching of non-collinear antiferromagnetic antiperovskites

G. Gurung, D.-F. Shao, and E. Y. Tsymbal

Rapid Communications

Spin-torque switching of noncollinear antiferromagnetic antiperovskites

Gautam Gurung, Ding-Fu Shao [*], and Evgeny Y. Tsymbal [†]
Department of Physics and Astronomy & Nebraska Center for Materials and Nanoscience, University of Nebraska, Lincoln, Nebraska 68588-0299, USA

(Received 13 January 2020; revised manuscript received 26 March 2020; accepted 26 March 2020; published 17 April 2020)

Antiferromagnetic (AFM) spintronics exploits the Néel vector as a state variable for novel electronic devices. Recent studies have demonstrated that the Néel vector can be switched by a spin-orbit torque. These studies however are largely limited to *collinear* antiferromagnets of proper magnetic space-group symmetry. There is, however, a large group of high-temperature *noncollinear* antiferromagnets, which are suitable for such switching. Here, we predict that spin torque can be efficiently used to switch a noncollinear AFM order in antiperovskite materials. Based on first-principles calculations and atomistic spin-dynamics modeling, we show that in antiperovskites $A\mathrm{NMn_3}$ (A = Ga, Ni, etc.) with the AFM Γ_{4g} ground state, the AFM order can be switched on the picosecond timescale using a spin torque generated by a spin current. The threshold switching current density can be tuned by the $A\mathrm{NMn_3}$ stoichiometry engineering, changing the magnetocrystalline anisotropy. The Γ_{4g} AFM phase supports a sizable anomalous Hall effect, which can be used to detect the spin-torque switching of the AFM order. The predicted ultrafast switching dynamics and the efficient detection of the AFM order state make noncollinear magnetic antiperovskites a promising material platform for AFM spintronics.

DOI: 10.1103/PhysRevB.101.140405

Antiferromagnetic (AFM) spintronics is a frontier research field, which has recently emerged as a subfield of spintronics, where an AFM order parameter also known as the Néel vector is exploited to control spin-dependent transport properties. Due to being robust against magnetic perturbations, producing no stray fields, and exhibiting ultrafast dynamics, antiferromagnets are promising candidates to replace ferromagnets in spintronic devices for information processing and storage [1–3]. To realize this potential, however, new schemes to write and read the information, which is stored in the AFM Néel vector, are required. The absence of net magnetization in antiferromagnets makes the realization of these schemes more challenging compared to their ferromagnetic counterparts.

Recent studies have shown that manipulation of the AFM Néel vector can be achieved by passing an electric current across a metallic collinear antiferromagnet of certain magnetic group symmetry. For example, in the antiferromagnets, such as CuMnAs [4] and $\mathrm{Mn_2Au}$ [5], where the space-inversion symmetry is broken but the two spin sublattices form space-inversion partners, the inverse spin galvanic effect produces staggered fieldlike spin torque on different sublattices [6–8]. When the electric current exceeds the critical value, this leads to switching of the Néel vector [4,5]. In the bilayer heterostructures, such as NiO/Pt [9,10] or $\mathrm{Mn_2Au}$/Pt [11], switching of the Néel vector can be achieved as a result of the antidamping spin torque produced by an injected spin current due to the spin-Hall effect. The detection of the AFM Néel vector in these structures is usually performed using anisotropic magnetoresistance (AMR) [12–14] or spin-Hall magnetoresistance (SMR) effects [15–18]. However, very small magnitudes of these effects (usually <1%) limit possible miniaturization and readout speed of these devices. Also, some of the observed magnetoresistive phenomena could have been an artifact of the large writing currents and the associated thermal effects, rather than the Néel vector switching [19].

Using the anomalous Hall effect (AHE) [20] may be a more promising way to realize a detection scheme of the AFM order parameter [21]. In this regard, *noncollinear* AFM materials [22] could provide a viable alternative to their collinear counterparts. Recent studies have shown that a number of high-temperature noncollinear antiferromagnets, such as $\mathrm{Mn_3}X$ (X = Ga, Ge, Sn, or Ir) [23–28] and antiperovskite $A\mathrm{NMn_3}$ (A = Ga, Zn, Ag, or Ni) [29–31] exhibit large anomalous Hall conductivities (AHC). Due to the AHC being odd with respect to time-reversal symmetry, reversal of the Néel vectors [32] in these compounds is expected to change sign of the AHE that can be used as an efficient detection scheme of the AFM order using the standard Hall measurements.

Switching of the AFM order in these noncollinear antiferromagnets can be achieved using a spin torque. It was argued that the magnetic structure of a noncollinear antiferromagnet can be dynamically controlled by injecting a spin current [33]. Using a simple two-dimensional model of a chiral antiferromagnet described by a single Kagomé layer, it was shown that spin structure can be rotated in the in plane by spin-transfer torque [34]. Very recently, it was predicted that the injected spin current, when it is polarized perpendicular to the triangular plane, can drive a translational motion of a domain wall in the Γ_{4g}- type antiferromagnet [35].

These modeling results provide important insights into the spin-torque driven magnetization dynamics in noncollinear antiferromagnets. However, a realistic description of the AFM

[*] dfshao@unl.edu
[†] tsymbal@unl.edu

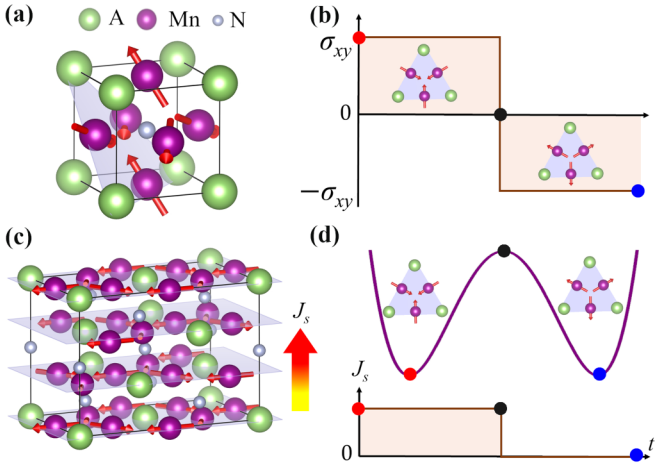

FIG. 1. (a) A cubic unit cell of antiperovskite ANMn$_3$ in the noncollinear AFM Γ_{4g} state. Red arrows denote the Mn magnetic moments. (b) The sign change of the anomalous Hall conductivity σ_{xy} induced by AFM order switching. The insets show magnetic configurations of ANMn$_3$ in the (111) plane. (c) The orthorhombic supercell of ANMn$_3$ used for the modeling of spin dynamics. Spin current J_s along the [111] direction exerts a spin torque on the magnetic moments of ANMn$_3$. (d) The switching process of the AFM order driven by the spin torque. The spin torque rotates the magnetic moments of the AFM Γ_{4g} phase away from their initial energy minimum through the metastable AFM Γ_{5g} phase. After overcoming the magnetic anisotropy barrier and releasing the current, the system relaxes to another minimum with the reversed AFM order.

order switching based on the magnetic properties of these antiferromagnets obtained from first principles is missing. In this work, we combine density-functional theory (DFT) calculations and atomistic spin-dynamics modeling based on the Landau-Lifshitz Gilbert-Slonczewski (LLGS) equation [36], and predict that the spin torque can efficiently control the noncollinear AFM order in antiperovskite materials. We demonstrate that in antiperovskites ANMn$_3$ (A = Ga, Ni, etc.), the AFM order of the Γ_{4g} ground state can be switched on the picosecond scale by a spin current. The threshold switching current density can be tuned by the ANMn$_3$ stoichiometry engineering that changes the magnetocrystalline anisotropy. The anomalous Hall effect then can be used to detect the spin-torque switching of the AFM order [37–47].

Antiperovskite compounds have the perovskite structure, where the cation and the anion interchange their positions [Fig. 1(a)]. The 3d transition-metal based intermetallic compounds AXM_3 (A is usually the main group element; X is the nonmetal element such as C, N; M is the 3d transition-metal element) is the most investigated antiperovskite material family. A special interest has been attracted to Mn-based antiperovskite nitrides ANMn$_3$ (A = Ga, Ni, Cu, Zn, etc.), where the AFM coupling within the frustrated Kagomé lattice in the (111) plane results in a noncollinear alignment of the magnetic moments in the AFM phases, such as Γ_{4g} [Fig. 1(a)] and Γ_{5g} [where all the Mn magnetic moments are rotated by 90° in the (111) plane]. These noncollinear AFM orderings lead to various functionalities such as magnetovolume [22,48,49], magnetocaloric [50,51], piezomagnetic [52–54], and magnetoelectric [55,56] effects.

Recently, the AHE has been predicted theoretically and confirmed experimentally in Mn-based antiperovskite nitrides with the Γ_{4g} AFM order [29–31,57,58]. Due to the AHC being odd with respect to the time-reversal symmetry operation, reversal of the AFM order in the Γ_{4g}-type antiperovskites is expected to change sign of the AHE [Fig. 1(b)]. This provides an efficient approach to distinguish between the two reversed AFM states in the Γ_{4g}-phase compounds. Thus, demonstrating a feasible method to switch between the two AFM states in the Γ_{4g} compounds would open a promising direction in AFM spintronics based on the AHE readout.

Here, we explore spin-torque switching of the AFM order in antiperovskite compounds exhibiting the Γ_{4g} noncollinear antiferromagnetism. We consider an antiperovskite thin film stacked in the (111) plane with the Mn magnetic moments aligned noncollinear in this plane due to the AFM exchange coupling. The magnetic dynamics is induced by spin current J_s injected along the [111] direction, as shown in Fig. 1(c). The spin current may be carried by a spin-polarized charge current from an adjacent ferromagnetic layer or may be produced by an adjacent heavy-metal layer due to the spin-Hall effect. The spin current J_s exerts a spin-transfer torque rotating the Mn magnetic moments in the (111) plane. The related magnetization dynamics is determined by the LLGS equation [59–61]:

$$\frac{\partial \vec{m}_i}{\partial t} = -\gamma(\vec{m}_i \times \vec{H}_i) + \alpha_G\left(\vec{m}_i \times \frac{\partial \vec{m}_i}{\partial t}\right) + \gamma\left(\vec{m}_i \times \vec{H}_i^s\right). \quad (1)$$

Here α_G is the Gilbert damping constant, γ is the gyromagnetic ratio, $\vec{m}_i = \frac{\vec{M}_i}{|\vec{M}_i|}$ is the unit magnetization vector for each sublattice with the magnetization $\vec{M}_i$. The magnetic field $\vec{H}_i = -\frac{1}{\mu}\frac{\partial H}{\partial \vec{m}_i}$ is determined by the spin Hamiltonian:

$$H = -\sum_{i \neq j} J_{ij}\vec{m}_i \cdot \vec{m}_j - K\sum_i (\hat{n}_i \cdot \vec{m}_i)^2, \quad (2)$$

where μ is the magnetic moment of a Mn atom, J_{ij} is the exchange coupling energy between sublattices, K is the magnetic anisotropy energy per Mn atom, and $\hat{n}_i$ is the direction of the easy axis for each sublattice. $\vec{H}_i^s = h_s(\vec{m}_i \times \vec{p}_s)$ is the effective magnetic field produced by the spin current J_s with the spin polarization along the $\vec{p}_s$ direction. The coefficient h_s is given by $h_s = \frac{\hbar J_s}{eLM}$, where $M = |\vec{M}_i|$ is the magnitude of the sublattice magnetization, e is the electronic charge, $\hbar$ is the Planck's constant, L is thickness of the sample. This effective field generates the spin torque $\sim \vec{m}_i \times \vec{H}_i^s$, which drives the magnetization dynamics.

To reverse the AFM order, all the moments need to be rotated by 180° within the horizontal plane [Fig. 1(d)]. If $\vec{p}_s$ is along an in-plane direction, the induced out-of-plane field $\vec{H}_i^s$ will have a tendency to reorient the moments out of plane. This will produce an additional parallel magnetic component which is energetically unfavorable due to the intrinsic AFM exchange coupling between the moments. On the other hand, if $\vec{p}_s$ is along the out-of-plane direction, i.e., $\vec{p}_s = \hat{z}$, the induced field $\vec{H}_i^s = h_s(\vec{m}_i \times \hat{z})$ is along the in-plane direction perpendicular to $\vec{m}_i$ [black arrows in Fig. 2(a)]. In this case, the staggered field $\vec{H}_i^s$ will rotate the magnetic moments in three sublattices nearly uniformly, not affecting the 120° angles between the nearest magnetic moments. This will not

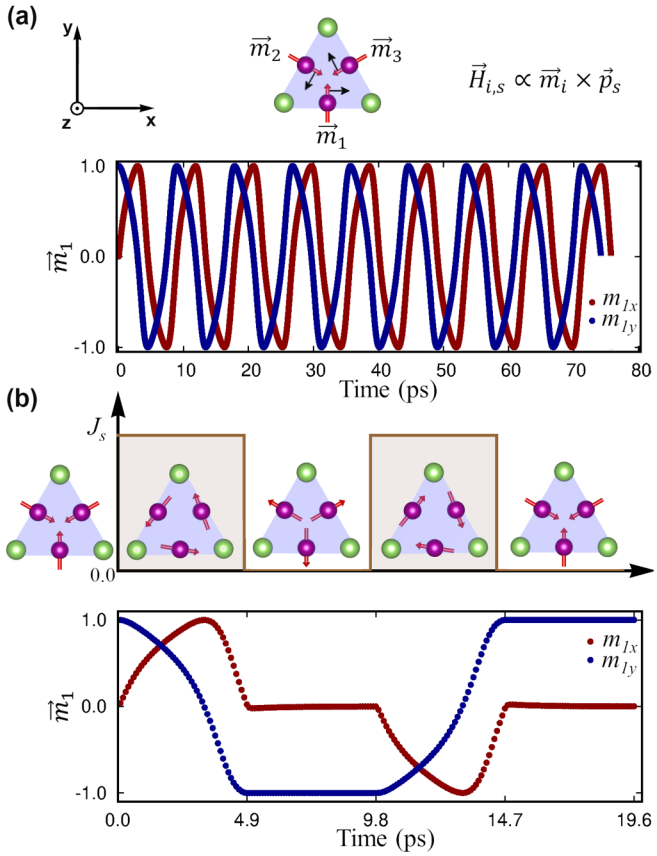

FIG. 2. Spin dynamics in antiperovskite $NiNMn_3$. (a) Top panel: schematic of effective magnetic field $\vec{H}_i^s$ (black arrows) on the three sublattices $\vec{m}_1$, $\vec{m}_2$, and $\vec{m}_3$ generated by spin current J_s with the spin polarization $\vec{p}_s$ along the z direction. Bottom panel: time-dependent variations of the x- and y components of $\vec{m}_1$ during the application of spin current $J_s = 1.8 \times 10^{12}$ A/m^2. (b) Top panel: schematic of the spin-torque switching process induced by two spin-current pulses. Bottom panel: time-dependent variations of the x- and y components of $\vec{m}_1$ driven by applying the two spin-current pulses of 4.9 ps in duration.

cost the exchange energy and thus is more favorable for the switching. Therefore, below we consider the spin-torque switching driven by spin current J_s with the spin polarization $\vec{p}_s$ along the $\hat{z}$ direction.

The atomistic modeling of the spin-torque dynamics is performed using an ANMn$_3$ (111) slab of thickness $L = 6$ nm which consists of periodically repeated supercells [Fig. 1(c)]. Specifically, we consider NiNMn$_3$, an antiperovskite metal, which AFM Γ_{4g} order and nonvanishing AHE effect near room temperature have been confirmed recently [30,57]. Consistent with the experiments, our DFT calculation shows that the Γ_{4g} order with negligible net magnetization has the lowest energy among the tested magnetic states in NiNMn$_3$. The parameters in Eq. (2) for NiNMn$_3$ are obtained from our DFT calculations. We found that each Mn atom has the moment of $2.76\mu_B$ and Ni atom does not have the local magnetic moment. The exchange constant J_{ij} is found to be -24 meV, using the energy-mapping method [62]. Reversal of the Γ_{4g} magnetic structure by 180° rotation of all magnetic moments about the [111] axis passes through the Γ_{5g} magnetic structure (90° rotation), which has higher energy due to magnetic anisotropy [Fig. 1(d)]. By calculating the energy difference between the Γ_{5g} and Γ_{4g} phases, we find that the magnetic anisotropy constant $K = (E_{5g} - E_{4g})/3 \approx 0.03$ meV per Mn atom. The damping constant α_G has been found experimentally to be in the range of 0.05 to 0.28 for similar noncollinear magnets [63,64]. In our modeling, we assume $\alpha_G = 0.1$ and gyromagnetic ratio $\gamma = 1.76 \times 10^{11}$ T^{-1} s^{-1}.

Figure 2(a) (top panel) shows the initial magnetic configuration, where the magnetic moments $\vec{m}_1$, $\vec{m}_2$, and $\vec{m}_3$ for the three sublattices point toward the center of the triangle formed by the nearest Mn atoms. In order to track the simulated spin-torque switching process, we observe variation of $\vec{m}_1$, which initially has zero x component (m_{1x}) and maximum y component (m_{1y}). Figure 2(a) (bottom panel) shows the rotation of $\vec{m}_1$ due to the spin torque produced by spin-current density $J_s = 1.8 \times 10^{12}$ A/m^2: when the current is turned on, m_{1x} and m_{1y} start to oscillate, revealing the clockwise rotation of the moments. The time period of these oscillations is $\tau \approx 9.8$ ps, which corresponds to the frequency of $f \approx 0.1$THz. The observed oscillation frequency qualitatively agree with that predicted in Ref. [33], i.e., $f \approx \frac{1}{4\pi\sqrt{3}} \frac{J_s}{J_c} \frac{\gamma K}{\alpha_G \mu}$, where J_c is the critical current density (see discussion below). We note that the predicted AFM dynamics may be interesting for the development of compact generators of coherent radiation in the Thz frequency range, which are important for different technological applications [65–67].

The 180° rotation of the moments can be achieved by application of a spin-current pulse, which duration is a half time of the oscillation period, i.e., $\tau/2 \approx 4.9$ ps. As shown in Fig. 2(b), applying such a pulse to the original magnetic configuration of NiNMn$_3$, where all three Mn magnetic moments $\vec{m}_1$, $\vec{m}_2$, and $\vec{m}_3$ are pointing to the center of the triangle formed by the nearest Mn atoms, switches $\vec{m}_1$, $\vec{m}_2$, and $\vec{m}_3$ to be pointing away from the center of the triangle. The switching occurs through an intermediate Γ_{5g} phase where the magnetic moments are aligned in a vortex. Applying a 4.9-ps pulse again switches the magnetic structure back to the initial configuration. These results demonstrate a possibility of an ultrafast spin-torque switching of the AFM order in NiNMn$_3$.

The spin current is produced either by a spin-polarized charge current or a charge current resulting in the spin-Hall effect. Since a large charge current generates Joule heat and thus is energy consuming, it is desirable to reduce its density and hence J_s required for the spin-torque switching. The major factor influencing J_s is the anisotropy energy [33,68]. In order to reorient Mn magnetic moments, the Zeeman energy μh_s of the magnetic moment in the effective field $\vec{H}_i^s$ generated by J_s should overcome the anisotropy energy K, i.e., $\mu h_s > K$. This condition leads to the critical current density $J_c = \frac{KLe}{\hbar V}$, where V is the volume of the cubic unit cell of NiNMn$_3$. This result for J_c is identical to that obtained in Ref. [33]. Since J_c is proportional to K, reducing the magnetic anisotropy is expected to reduce the critical current density.

This expectation is confirmed by our atomistic modeling of the spin-torque switching of NiNMn$_3$, where we fix all the parameters but vary the magnetic anisotropy constant K. As expected and seen from Fig. 3(a), with decreasing K the

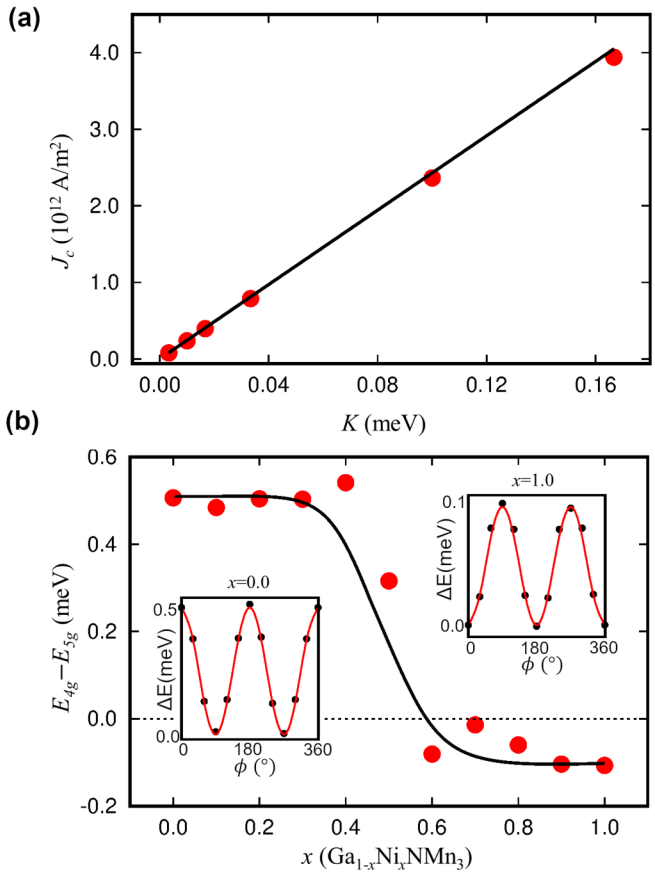

FIG. 3. (a) Critical current density J_c for switching of the AFM order in $ANMn_3$ antiperovskite as a function of the anisotropy energy. The red dots are J_c obtained by the atomistic spin dynamics modeling. The solid black line is obtained from $J_c = \frac{KLe}{\hbar V}$. (b) The energy difference between the Γ_{4g} and Γ_{5g} magnetic configurations in $Ga_{1-x}Ni_xNMn_3$. The insets show the energy as a function of rotation angle ϕ of the magnetic moments around the [111] axis in $Ga_{1-x}Ni_xNMn_3$ for $x = 0$ ($GaNMn_3$) and $x = 1$ ($NiNMn_3$), where $\Delta E = E_{4g} - E(\phi)$.

J_c decreases linearly. According to our modeling results, the critical current density J_c is reduced to about 10^{10} A/m^2 if the anisotropy constant K is 0.01 meV per Mn atom. The calculated critical current density is in agreement with that predicted by the simple estimate $J_c = \frac{KLe}{\hbar V}$ [see the solid line in Fig. 3(a)].

The magnetic anisotropy of the antiperovskite can be controlled by chemical doping. There are a number of antiperovskites with the AFM Γ_{5g} order, such as $GaNMn_3$. Therefore, a doped compound $Ga_{1-x}Ni_xNMn_3$ is expected to exhibit the ground Γ_{5g} state in the Ga-rich phase and the Γ_{4g} state in the Ni-rich phase. At the intermediate doping x, there should be a transition point between these two phases, where the magnetic anisotropy is zero. Figure 3(b) shows the calculated energy difference between the Γ_{5g} and Γ_{4g} magnetic orderings as a function of doping x. Consistent with experimental results, we find that the ground state is Γ_{5g} for $GaNMn_3$ ($x = 0$) and Γ_{4g} for $NiNMn_3$ ($x = 1$). There is a transition between the two phases for $x \approx 0.58$. At this region, the magnetic anisotropy is strongly reduced, and the small critical current density $\sim 10^{10}$ A/m^2 is expected for spin-torque switching of the AFM order.

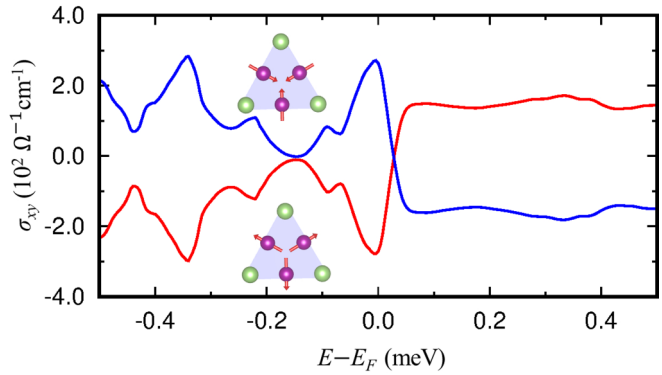

FIG. 4. Calculated anomalous Hall conductivity (AHC)σ_{xy} of antiperovskite $Ga_{0.42}Ni_{0.58}NMn_3$ with the AFM Γ_{4g} order as a function of energy. The red and blue lines denote the AHC for the two AFM states with reversed magnetic structure shown in the insets.

Switching of the AFM order in the Γ_{4g} phase can be detected by measuring the anomalous Hall conductivity:

$$\sigma_{\alpha\beta} = -\frac{e^2}{\hbar}\int_{BZ}\frac{d^3\vec{k}}{(2\pi)^3}\Omega_{\alpha\beta}(\vec{k}), \tag{3}$$

where $\Omega_{\alpha\beta} = \sum_n f_n(\vec{k})\Omega_{n,\alpha\beta}(\vec{k})$ is the sum of the Berry curvatures $\Omega_{n,\alpha\beta}(\vec{k})$ corresponding the individual bands n, $f_n(\vec{k})$ is the Fermi distribution function, and indices (α, β) denote Cartesian coordinates. The expression for the Berry curvature $\Omega_{n,\alpha\beta}(\vec{k})$ is given by [20,69]

$$\Omega_{n,\alpha\beta}(\vec{k}) = -2i\hbar^2\sum_{\mathrm{m}\neq\mathrm{n}}\frac{\langle\psi_{n,\vec{k}}|v_\alpha|\psi_{\mathrm{m},\vec{k}}\rangle\langle\psi_{m,\vec{k}}|v_\beta|\psi_{n,\vec{k}}\rangle}{\left(E_m(\vec{k}) - E_n(\vec{k})\right)^2}, \tag{4}$$

where $\psi_{n,\vec{k}}$ is the Bloch function and $\vec{v}$ is the velocity operator. The Berry curvature is odd under certain symmetry operations, i.e., $\hat{O}\Omega_n(\vec{k}') = -\Omega_n(\vec{k})$, where $\hat{O}$ is a symmetry operation such as time-reversal symmetry or mirror symmetry [69,70]. In the Γ_{4g} AFM state, there is no such symmetry operation $\hat{O}$ with respect to which Ω_n is odd [29]. Therefore, a finite value can be obtained according to Eq. (4), leading to the appearance of the anomalous Hall effect. Figure 4 shows the calculated AHC σ_{xy} of $Ga_{1-x}Ni_xNMn_3$ as a function of energy for $x = 0.58$. We find sizable $\sigma_{xy} = 260\ \Omega^{-1}\ \mathrm{cm}^{-1}$ at the Fermi energy. Rotating the magnetic moments around the [111] axis changes the magnetic space group and thus the band structure, which affects the magnitude of σ_{xy} [71]. As shown in Supplemental Material [36], σ_{xy} decreases when the moments are rotated away from their initial alignment in the Γ_{4g} state, and vanishes when the moments are aligned in the Γ_{5g} state. The AHC changes sign with reversal of the AFM order, as shown in Fig. 4.

We note that the AFM order can be switched in the antiperovskite $ANMn_3$ films layered in the plane different from (111). As long as the spin-polarization of the spin current has the component perpendicular to the (111) plane, the spin-torque switching of the noncollinear AFM order can be achieved. The spin current can be generated from a nonmetal bottom layer through the spin-Hall effect. Recently, such a spin-Hall

torque switching has been reported in the $GaNMn_3$ (001)/Pt bilayer structure [72]. In this experiment AFM switching was detected using a conventional AMR effect, since the noncollinear AFM Γ_{5g} phase in Mn_3GaN does not support the AHE [29]. The sign change of the AHC in noncollinear AFM antiperovskites exhibiting the AFM Γ_{4g} phase, which is demonstrated in our paper, is advantageous for the AFM order detection compared to the conventional AMR and SMR measurements.

In conclusion, we have predicted a possibility of spin-torque switching of the noncollinear AFM order in Mn-based antiperovskite nitrides, such as $NiNMn_3$. We have shown that this switching can be achieved on the picosecond timescale using a spin-current density feasible in experiment. The critical current density for AFM switching can be reduced by controlling the magnetocrystalline anisotropy through the stoichiometry engineering. For the antiperovskite compound $Ga_{1-x}Ni_xNMn_3$ with $x \approx 0.58$, we have predicted the critical spin-current density $J_c \sim 10^{10}$ A/m^2 and sizable anomalous Hall conductivity $\sigma_{xy} = 260\ \Omega^{-1}\,\mathrm{cm}^{-1}$. The anomalous Hall conductivity changes sign with the AFM switching and hence can be used for the AFM order detection. Our prediction offers a material platform based on noncollinear AFM antiperovskites to realize both the efficient manipulation and detection of the AFM order, which is promising for the next generation of the AFM spintronic devices.

This research was supported by the National Science Foundation (NSF) through Nebraska MRSEC (Grant No. DMR-1420645) and DMREF (Grant No. DMR-1629270) programs. Computations were performed at the University of Nebraska Holland Computing Center. The figures are created using VESTA [73] and GNUPLOT [74].

[1] T. Jungwirth, X. Marti, P. Wadley, and J. Wunderlich, Antiferromagnetic spintronics, Nat. Nanotechnol. **11**, 231 (2016).
[2] V. Baltz, A. Manchon, M. Tsoi, T. Moriyama, T. Ono, and Y. Tserkovnyak, Antiferromagnetic spintronics, Rev. Mod. Phys. **90**, 015005 (2018).
[3] T. Jungwirth, J. Sinova, A. Manchon, X. Marti, J. Wunderlich, and C. Felser, The multiple directions of antiferromagnetic spintronics, Nat. Phys. **14**, 200 (2018).
[4] P. Wadley, B. Howells, J. Železný, C. Andrews, V. Hills, R. P. Campion, V. Novák, K. Olejník, F. Maccherozzi, S. S. Dhesi, S. Y. Martin, T. Wagner, J. Wunderlich, F. Freimuth, Y. Mokrousov, J. Kuneš, J. S. Chauhan, M. J. Grzybowski, A. W. Rushforth, K. W. Edmonds, B. L. Gallagher, and T. Jungwirth, Electrical switching of an antiferromagnet, Science **351**, 587 (2016).
[5] S. Y. Bodnar, L. Šmejkal, I. Turek, T. Jungwirth, O. Gomonay, J. Sinova, A. A. Sapozhnik, H.-J. Elmers, M. Kläui, and M. Jourdan, Writing and reading antiferromagnetic Mn_2Au by Néel spin-orbit torques and large anisotropic magnetoresistance, Nat. Commun. **9**, 348 (2018).
[6] J. Železný, H. Gao, K. Výborný, J. Zemen, J. Mašek, A. Manchon, J. Wunderlich, J. Sinova, and T. Jungwirth, Relativistic Néel-Order Fields Induced by Electrical Current in Antiferromagnets, Phys. Rev. Lett. **113**, 157201 (2014).
[7] J. Železný, H. Gao, A. Manchon, F. Freimuth, Y. Mokrousov, J. Zemen, J. Mašek, J. Sinova, and T. Jungwirth, Spin-orbit torques in locally and globally noncentrosymmetric crystals: Anti-ferromagnets and ferromagnets, Phys. Rev. B **95**, 014403 (2017).
[8] A. Manchon, J. Zelezný, I. M. Miron, T. Jungwirth, J. Sinova, A. Thiaville, K. Garello, and P. Gambardella, Current-induced spin-orbit torques in ferromagnetic and antiferromagnetic systems, Rev. Mod. Phys. **91**, 035004 (2019).
[9] X. Z. Chen, R. Zarzuela, J. Zhang, C. Song, X. F. Zhou, G. Y. Shi, F. Li, H. A. Zhou, W. J. Jiang, F. Pan, and Y. Tserkovnyak, Antidamping Torque-Induced Switching in Biaxial Antiferromagnetic Insulators, Phys. Rev. Lett. **120**, 207204 (2018).
[10] T. Moriyama, K. Oda, T. Ohkochi, M. Kimata, and T. Ono, Spin torque control of antiferromagnetic moments in NiO, Sci. Rep. **8**, 14167 (2018).
[11] X. F. Zhou, X. Z. Chen, J. Zhang, F. Li, G. Y. Shi, Y. M. Shun, M. S. Saleem, Y. F. You, F. Pan, and C. Song, From Fieldlike Torque to Antidamping Torque in Antiferromagnetic Mn_2Au, Phys. Rev. Appl. **11**, 054030 (2019).
[12] B. G. Park, J. Wunderlich, X. Martí, V. Holý, Y. Kurosaki, M. Yamada, H. Yamamoto, A. Nishide, J. Hayakawa, H. Takahashi, A. B. Shick, and T. Jungwirth, A spin-valve-like magnetoresistance of an antiferromagnet-based tunnel junction, Nat. Mater. **10**, 347 (2011).
[13] X. Martí, B. G. Park, J. Wunderlich, H. Reichlová, Y. Kurosaki, M. Yamada, H. Yamamoto, A. Nishide, J. Hayakawa, H. Takahashi, and T. Jungwirth, Electrical Measurement of Antiferromagnetic Moments in Exchange-Coupled IrMn/NiFe Stacks, Phys. Rev. Lett. **108**, 017201 (2012).
[14] Y. Y. Wang, C. Song, B. Cui, G. Y. Wang, F. Zeng, and F. Pan, Room-Temperature Perpendicular Exchange Coupling and Tunneling Anisotropic Magnetoresistance in an Antiferromagnet-Based Tunnel Junction, Phys. Rev. Lett. **109**, 137201 (2012).
[15] H. Nakayama, M. Althammer, Y.-T. Chen, K. Uchida, Y. Kajiwara, D. Kikuchi, T. Ohtani, S. Geprägs, M. Opel, S. Takahashi, R. Gross, G. E. W. Bauer, S. T. B. Goennenwein, and E. Saitoh, Spin Hall Magnetoresistance Induced by a Nonequilibrium Proximity Effect, Phys. Rev. Lett. **110**, 206601 (2013).
[16] H. Wang, D. Hou, Z. Qiu, T. Kikkawa, E. Saitoh, and X. Jin, Antiferromagnetic anisotropy determination by spin Hall magnetoresistance, J. Appl. Phys. **122**, 083907 (2017).
[17] D. Hou, Z. Qiu, J. Barker, K. Sato, K. Yamamoto, S. Vélez, J. M. Gomez-Perez, L. E. Hueso, F. Casanova, and E. Saitoh, Tunable Sign Change of Spin Hall Magnetoresistance in Pt/NiO/YIG Structures, Phys. Rev. Lett. **118**, 147202 (2017).
[18] L. Baldrati, A. Ross, T. Niizeki, C. Schneider, R. Ramos, J. Cramer, O. Gomonay, M. Filianina, T. Savchenko, D. Heinze, A. Kleibert, E. Saitoh, J. Sinova, and M. Kläui, Full angular

dependence of the spin Hall and ordinary magnetoresistance in epitaxial antiferromagnetic NiO(001)/Pt thin films, Phys. Rev. B **98**, 024422 (2018).

[19] C. C. Chiang and S. Y. Huang, D. Qu, P. H. Wu, and C. L. Chien, Absence of Evidence of Electrical Switching of the Antiferromagnetic Néel Vector, Phys. Rev. Lett. **123**, 227203 (2019).

[20] N. Nagaosa, J. Sinova, S. Onoda, A. H. MacDonald, and N. P. Ong, Anomalous Hall effect, Rev. Mod. Phys. **82**, 1539 (2010).

[21] T. Kosub, M. Kopte, R. Hühne, P. Appel, B. Shields, P. Maletinsky, R. Hübner, M. O. Liedke, J. Fassbender, O. G. Schmidt, and D. Makarov, Purely antiferromagnetic magnetoelectric random access memory, Nat. Commun. **8**, 13985 (2017).

[22] D. Fruchart and E. F. Bertaut, Magnetic studies of the metallic perovskite-type compounds of manganese. J. Phys. Soc. Jpn. **44**, 781 (1978).

[23] H. Chen, Q. Niu, and A. H. MacDonald, Anomalous Hall Effect Arising from Noncollinear Antiferromagnetism, Phys. Rev. Lett. **112**, 017205 (2014).

[24] J. Kübler and C. Felser, Non-collinear antiferromagnets and the anomalous Hall effect, Europhys. Lett. **108**, 67001 (2014).

[25] S. Nakatsuji, N. Kiyohara, and T. Higo, Large anomalous Hall effect in a non-collinear antiferromagnet at room temperature, Nature (London) **527**, 212 (2015).

[26] A. K. Nayak, J. E. Fischer, Y. Sun, B. Yan, J. Karel, A. C. Komarek, C. Shekhar, N. Kumar, W. Schnelle, J. Kübler, C. Felser, and S. P. P. Parkin, Large anomalous Hall effect driven by a nonvanishing Berry curvature in the noncollinear antiferromagnet Mn_3Ge, Sci. Adv. **2**, e1501870 (2016).

[27] Y. Zhang, Y. Sun, H. Yang, J. Železný, S. P. P. Parkin, C. Felser, and B. Yan, Strong anisotropic anomalous Hall effect and spin Hall effect in the chiral antiferromagnetic compounds Mn_3X (X = Ge, Sn, Ga, Ir, Rh, and Pt), Phys. Rev. B **95**, 075128 (2017).

[28] N. Kiyohara, T. Tomita, and S. Nakatsuji, Giant Anomalous Hall Effect in the Chiral Antiferromagnet Mn_3Ge, Phys. Rev. Appl. **5**, 064009 (2016).

[29] G. Gurung, D.-F. Shao, T. R. Paudel, and E. Y. Tsymbal, Anomalous Hall conductivity of non-collinear magnetic antiperovskites, Phys. Rev. Mater. **3**, 044409 (2019).

[30] D. Boldrin, I. Samathrakis, J. Zemen, A. Mihai, B. Zou, B. Esser, D. McComb, P. Petrov, H. Zhang, and L. F. Cohen, The anomalous Hall effect in non-collinear antiferromagnetic Mn_3NiN thin films, Phys. Rev. Mater. **3**, 094409 (2019).

[31] X. Zhou, J.-P. Hanke, W. Feng, F. Li, G.-Y. Guo, Y. Yao, S. Blügel, and Y. Mokrousov, Spin-order dependent anomalous Hall effect and magneto-optical effect in the noncollinear antiferromagnets Mn_3XN with X = Ga, Zn, Ag, or Ni, Phys. Rev. B **99**, 104428 (2019).

[32] There are several Néel vectors describing an AFM order in noncollinear antiferromagnets. Switching of the antiferromagnet implies reversal of all of them. Below we refer to this process as "AFM order switching."

[33] H. V. Gomonay and V. M. Loktev, Spin transfer and current-induced switching in antiferromagnets, Phys. Rev. B **81**, 144427 (2010).

[34] H. Fujita, Field-free, spin-current control of magnetization in non-collinear chiral antiferromagnets, Phys. Status Solidi RRL **11**, 1600360 (2017).

[35] Y. Yamane, O. Gomonay, and J. Sinova, Dynamics of noncollinear antiferromagnetic textures driven by spin current injection, Phys. Rev. B **100**, 054415 (2019).

[36] See Supplemental Material at http://link.aps.org/supplemental/10.1103/PhysRevB.101.140405 for the description of calculation methods, the magnetic ground state of $NiNMn_3$, and the influence of the moment rotation on the anomalous Hall conductivity, which includes Refs. [37–47].

[37] G. Kresse and D. Joubert, Fully unconstrained noncollinear magnetism within the projector augmented-wave method, Phys. Rev. B **59**, 1758 (1999).

[38] P. Giannozzi *et al.*, Quantum ESPRESSO: A modular and open-source software project for quantum simulations of materials, J. Phys. Condens. Matter **21**, 395502 (2009).

[39] P. E. Blöchl, Projected augmented-wave method, Phys. Rev. B **50**, 17953 (1994).

[40] D. Vanderbilt, Soft self-consistent pseudopotentials in a generalized eigenvalue formalism, Phys. Rev. B **41**, 7892 (1990).

[41] J. P. Perdew, K. Burke, and M. Ernzerhof, Generalized gradient approximation made simple, Phys. Rev. Lett. **77**, 3865 (1996).

[42] H. Rosner, R. Weht, M. D. Johannes, W. E. Pickett, and E. Tosatti, Superconductivity Near Ferromagnetism in $MgCNi_3$, Phys. Rev. Lett. **88**, 027001 (2001).

[43] R. F. L. Evans, W. J. Fan, P. Chureemart, T. A. Ostler, M. A. Ellis, and R. W. Chantrell, Atomistic spin model simulations of magnetic nanomaterials, J. Phys. Condens. Matter **26**, 103202 (2014).

[44] M. B. Nardelli, F. T. Cerasoli, M. Costa, S. Curtarolo, R. De Gennaro, M. Fornari, L. Liyanage, A. Supka, and H. Wang, PAOFLOW: A utility to construct and operate on *ab-initio* Hamiltonians from the projections of electronic wavefunctions on atomic orbital bases, including characterization of topological materials, Comput. Mat. Sci. **143**, 462 (2017).

[45] L. A. Agapito, A. Ferretti, A. Calzolari, S. Curtarolo, and M. B. Nardelli, Effective and accurate representation of extended Bloch states on finite Hilbert spaces, Phys. Rev. B **88**, 165127 (2013).

[46] L. A. Agapito, S. Ismail-Beigi, S. Curtarolo, M. Fornari, and M. B. Nardelli, Accurate tight-binding Hamiltonian matrices from *ab-initio* calculations: Minimal basis sets, Phys. Rev. B **93**, 035104 (2016).

[47] J. R. Yates, X. Wang, D. Vanderbilt, and I. Souza, Spectral and Fermi surface properties from Wannier interpolation, Phys. Rev. B **75**, 195121 (2007).

[48] T. Kaneko, T. Kanomata, and K. Shirakawa, Pressure effect on the magnetic transition temperatures in the intermetallic compounds Mn_3MC (M = Ga, Zn and Sn), J. Phys. Soc. Jpn. **56**, 4047 (1987).

[49] K. Takenaka, M. Ichigo, T. Hamada, A. Ozawa, T. Shibayama, T. Inagaki, and K. Asano, Magnetovolume effects in manganese nitrides with antiperovskite structure, Sci. Tech. Adv. Mater. **15**, 015009 (2014).

[50] T. Tohei, H. Wada, and T. Kanomata, Negative magnetocaloric effect at the antiferromagnetic to ferromagnetic transition of Mn_3GaC, J. Appl. Phys. **94**, 1800 (2003).

[51] B. S. Wang, P. Tong, Y. P. Sun, X. Luo, X. B. Zhu, G. Li, X. D. Zhu, S. B. Zhang, Z. R. Yang, and W. H. Song, Large magnetic entropy change near room temperature in antiperovskite $SnCMn_3$, Europhys. Lett. **85**. 47004 (2009).

[52] P. Lukashev, R. F. Sabirianov, and K. Belashchenko, Theory of piezomagnetic effect in Mn-based antiperovskites, Phys. Rev. B **78**, 184414 (2008).

[53] J. Zemen, Z. Gercsi, and K. G. Sandeman, Piezomagnetism as a counterpart of the magnetovolume effect in magnetically frustrated Mn-based antiperovskite nitrides, Phys. Rev. B **96**, 024451 (2017).

[54] D. Boldrin, A. P. Mihai, B. Zou, J. Zemen, R. Thompson, E. Ware, B. V. Neamtu, L. Ghivelder, B. Esser, D. W. McComb, P. Petrov, and L. F. Cohen., Giant piezomagnetism in Mn_3NiN, ACS Appl. Mater. Int. **10**, 18863 (2018).

[55] P. Lukashev, K. D. Belashchenko, and R. F. Sabirianov, Large magnetoelectric effect in ferroelectric/piezomagnetic heterostructures, Phys. Rev. B **84**, 134420 (2011).

[56] D. F. Shao and G. Gurung, T. R. Paudel, and E. Y. Tsymbal, Electrically reversible magnetization at the antiperovskite/perovskite interface, Phys. Rev. Mater. **3**, 024405 (2019).

[57] K. Zhao, T. Hajiri, H Chen, R. Miki, H. Asano, and P. Gegenwart, Anomalous Hall effect in the noncollinear antiferromagnetic antiperovskite $Mn_3Ni_{1-x}Cu_xN$, Phys. Rev. B **100**, 045109 (2019).

[58] V. T. N. Huyen, M. T. Suzuki, K Yamauchi, and T. Oguchi, Topology analysis for anomalous Hall effect in the noncollinear antiferromagnetic states of Mn_3AN (A = Ni, Cu, Zn, Ga, Ge, Pd, In, Sn, Ir, Pt), Phys. Rev. B **100**, 094426 (2019).

[59] J. C. Slonczewski, Current-driven excitation of magnetic multilayers, J. Magn. Magn. Matter **159**, L1 (1996).

[60] Z. Li and S. Zhang, Magnetization dynamics with a spin-transfer torque, Phys. Rev. B **68**, 024404 (2003).

[61] S. Zhang, P. M. Levy, and A. Fert, Mechanisms of Spin-Polarized Current-Driven Magnetization Switching, Phys. Rev. Lett. **88**, 236601 (2002).

[62] H. J. Xiang, E. J. Kan, S. H. Wei, M.-H. Whagngbo, and X. G. Gong, Predicting the spin-lattice order of frustrated systems from first principles, Phys. Rev. B **84**, 224429 (2011).

[63] T. Schwarze, J. Waizner, M. Garst, A. Bauer, I. Stasinopoulos, H. Berger, C. Pfleiderer, and D. Grundler, Universal helimagnon and skyrmion excitations in metallic, semiconducting and insulating chiral magnets, Nat. Mater. **14**, 478 (2015).

[64] M. Beg, M. Albert, M.-A. Bisotti, D. Cortés-Ortuño, W. Wang, R. Carey, M. Vousden, O. Hovorka, C. Ciccarelli, C. S. Spencer, C. H. Marrows, and H. Fangohr, Dynamics of skyrmionic states in confined helimagnetic nanostructures, Phys. Rev. B **95**, 014433 (2017).

[65] B. Ferguson and X. Zhang, Materials for terahertz science and technology, Nat. Mater. **1**, 26 (2002).

[66] M. Tonouchi, Cutting-edge terahertz technology, Nat. Photonics **1**, 97 (2007).

[67] R. Kleiner, Filling the terahertz gap, Science **318**, 1254 (2007).

[68] O. V. Gomonay and V. M. Loktev, Using generalized Landau-Lifshitz equations to describe the dynamics of multi-sublattice antiferromagnets induced by spin-polarized current, Low Temp. Phys. **41**, 698 (2015).

[69] M. Gradhand, D. V. Fedorov, F. Pientka, P. Zahn, I. Mertig, and B. K. Györffy, First-principle calculations of the Berry curvature of Bloch states for charge and spin transport of electrons, J. Phys.: Condens. Matter **24**, 213202 (2012).

[70] M. V. Berry, Quantal phase factors accompanying adiabatic changes, Proc. R. Soc. A **392**, 45 (1984).

[71] M. P. Ghimire, J. I. Facio, J.-S. You, L. Ye, J. G. Checkelsky, S. Fang, E. Kaxiras, M. Richter, and J. van den Brink, Creating Weyl nodes and controlling their energy by magnetization rotation, Phys. Rev. Res. **1**, 032044(R) (2019).

[72] T. Hajiri, S. Ishino, K. Matsuura, and H. Asano, Electrical current switching of the noncollinear antiferromagnet Mn_3GaN, Appl. Phys. Lett. **115**, 052403 (2019).

[73] K. Momma and F. Izumi, VESTA: Athree-dimensional visualization system for electronic and structural analysis, J. Appl. Crystallogr. **41**, 653 (2008).

[74] T. Williams, C. Kelley, H. B. Broker, J. Campbell, R. Cunningham, D. Denholm, E. Elber, R. Fearick, C. Grammes, and L. Hart, GNUPLOT 4.5: An interactive plotting program, 2011, http://www.gnuplot.Info (2017).